Dalton Transactions

Accepted Manuscript

ROYAL SOCIETY OF CHEMISTRY

www.rsc.org/dalton

Preparation of a novel nanocomposite $NaLuF_4$: Gd, Yb, Tm@SiO_2@Ag@TiO_2 with high photocatalytic activity driven by simulated solar light

Dongguang Yin*, Lu Zhang, Xianzhang Cao, Zhiwen Chen, Jingxiu Tang, Yumin Liu,

Tingting Zhang, Minghong Wu*

School of Environmental and Chemical Engineering, Shanghai University, Shanghai 200444, China

ABSTRACT: A novel nanocomposite photocatalyst $NaLuF_4$: Gd, Yb, Tm@SiO_2@Ag @TiO_2 was developed for the first time. This composite material has a sandwich structure, including a $NaLuF_4$: Gd, Yb, Tm upconversion nanocrystals (UCNCs) core, a media shell of amorphous SiO_2 decorated with Ag nanoparticles, and an outer shell of anatase TiO_2. The designed new structure takes advantage of synergetic effect of UCNCs, Ag nanoparticles and TiO_2. The UCNCs absorb NIR light and transfer energy to TiO_2, which extended the light responsive range of TiO_2 to NIR region. The Ag nanoparticles not only enhance upconversion luminescence of the UCNCs, but also enhance light harvesting and improve charges separation of TiO_2. The results of photocatalytic applications show that the as-prepared catalyst has high photocatalytic activity. This work provides new insights into the fabrication of TiO_2-based nanocomposite photocatalyst with high catalytic efficiency through effective integration of upconversion material, noble metal and TiO_2 into a hetero-composite nanostructure.

KEYWORDS: $NaLuF_4$:Gd,Yb,Tm@SiO_2@Ag@TiO_2 Nanocomposite; Photocatalysis; Preparation; Improvement; Photocatalytic Activity.

1. INTRODUCTION

In recent years, water and air pollution has becoming a serious problem that attracted great attention all over the world.[1] Photocatalysis, a highly effective and environmental friendly technique using clean, safe and renewable solar energy, has been widely used for water and air purification.[2-5] Among all kinds of photocatalysts, TiO_2 photocatalysis has aroused great interest due to its high efficiency, extraordinary chemical stability, low cost and environmental friendly characters.[6-9] However, due to its large bandgap of ~ 3.2 eV, TiO_2 can only harvest UV light[10] that only possess ~5% of solar energy, whereas the percentages of visible and near-infrared (NIR) lights are about~49% and ~46%, respectively.[11] On the other hand, the photogenerated electorn-hole pairs in TiO_2 are easy to recombine.[12] These facts restrict its large scale application in environmental protection issues. Up to date, much effort have been made to improve photocatalytic activity of TiO_2 and expand its application by extending the photo responding range and inhibiting the recombination of electron-hole pairs. For example, surface modification,[13] structure optimization, and doping of the third element are the routine routes to extend the optical absorption of TiO_2.[14-17] Meanwhile, deposition of noble metals, coupling with narrow bandgap semiconductor, utilization of electron donors-acceptors and hole scavengers are typical approaches to restrict the recombination of photogenerated electron-hole pairs.[18-20] Although much progress has been made to extend the light harvesting region (mostly visible light region) and restrict charge recombination, it is still a big challenge to significantly enhance the efficiency of TiO_2 based photocatalysis. Moreover, even using the methods mentioned above, efficient NIR absorption for photocatalysis is still unreached yet, and the energy of the photogenerated electron-hole pairs excited by visible light are not powerful enough to decompose organic

pollutants completely.[10, 11, 21] Therefore, substantial improvement of photocatalytic activity of TiO_2 and large scale application of TiO_2-based photocatalysts to solve environmental and energy problems needs further innovational work.

In this work, we designed and synthesized a novel TiO_2-based nanocomposite photocatalyst. It has a sandwich structure, consisting of UCNCs of $NaLuF_4$: Gd, Yb, Tm as the core, amorphous SiO_2 as the media shell decorated with Ag nanoparticles, and anatase TiO_2 nanocrystals as the outer shell. $NaYF_4$-based UCNCs are well-known as efficient upconversion nanocrystals.[22-24] However, some studies including ours in recent year reported that $NaLuF_4$ is a better host material for UCNs compared to the $NaYF_4$-based nanocrystals.[25-28] The doped Gd^{3+} in the UCNCs may act as an intermediate through which the excited energy can migrate over the Gd^{3+} sublattice and consequently facilitate the energy transfer process in fluoride phosphor.[25, 29, 30] Moreover, the Gd^{3+} doping can promote the transformation of the UCNs from the cubic to the hexagonal phase, resulting in enhancing UCL.[9, 23, 27, 31] Based on these, we prepared $NaLuF_4$: Gd, Yb, Tm as the UCNCs to fabricate the composite photocatalyst. The designed structure of the composite photocatalyst is different from UCNCs@TiO_2 or UCNCs@SiO_2@TiO_2 core/shell nanostructures reported in previous literatures.[32-34] Based on the designed structure, the upconversion nanocrystals and Ag nanoparticles have a synergistic effect which can improve the photocatalytic activity of TiO_2 significantly. The UCNCs absorb NIR of solar and upconvert it into visible and UV light which is absorbed by TiO_2. The photogenerated electrons and holes excited by UV light have high capability of oxidation and reduction to degrade pollutants completely. The Ag nanoparticles take a very important role in the composite, which can not only enhance upconversion luminescence of the upconversion nanocrystals as well as light harvesting of the

TiO_2, but also improve charges separation of TiO_2.[35-37] This work provides new insight into the fabrication of TiO_2-based composite photocatalyst with high catalytic activity through artificial integration of UCNCs, noble metal Ag and TiO_2 into a hetero-nanostructure.

2. EXPERIMENTAL SECTION

2.1. MATERIALS

Rare earth oxides Lu_2O_3 (99.999%), Gd_2O_3 (99.999%), Yb_2O_3 (99.999%), and Tm_2O_3 (99.999%) were purchased from Shanghai Yuelong New Materials Co. Ltd. Oleic acid (OA) (>90%) and 1-octadecene (>90%), (3-Aminopropyl)triethoxysilane (APTES) (>98%), Titanium(IV) ethoxide (>98%), sodium carbonate, ethanol, octanol, Triton X-100, tetraethoxysilane (TEOS), $NH_3 \cdot H_2O$ (28 wt%), $AgNO_3$, trifluoroacetic acid, sodium citrate and cyclohexane were supplied from Sinopharm Chemical Reagent Co., Ltd. (Shanghai). Rhodamine B (RhB), and hydroxypropyl cellulose (HPC, Mw = 80,000) were purchased from Sigma-Aldrich. P25 (TiO_2, 99.5%) was purchased from Degussa Co. Ltd. (Germany). $Ln(CF_3COO)_3$ (Ln: Lu, Gd, Yb, Tm) precursors were prepared by dissolving the corresponding metal oxides in trifluoroacetic acid at elevated temperature.

2.2. Preparation of $NaLuF_4$: Gd, Yb, Tm

In typically, 10 mL each of the coordinating oleic acid (90%) ligand and the non-coordinating solvent 1-octadecene (90%) were added to the reaction vessel (Solution A). 2 mmol sodium trifluoroacetic acid (98%) and 1 mmol lanthanide trifluoroacetate precursors were added to the solution containing 5 ml oleic acid and 5 mL 1-octadecene (Solution B). Subsequently, both A and

B solutions were heated to 120° C under vacuum with magnetic stirring and kept for 30 min. Then the solution A was heated to 310℃ under N_2 gas atmosphere. After that, the solution B was added to the reaction vessel drop by drop at a rate of 1.5 mL/min. The mixture solution was maintained at this temperature and stirred vigorously for 1h, then cooled down to 80℃. The formed nanocrystals were precipitated from the solution with addition of excess of ethanol, and collected after centrifuging and washing with hexane/ethanol (1:1 v/v) for three times.

2.3. Preparation of $NaLuF_4$: Gd, Yb, Tm@SiO_2

First, 6.7 mL of octanol and 12 mL of Triton X-100 were dispersed in 50 mL of cyclohexane by sonication and stirring. Then, 5 mL of (0.1 mmol/mL) UCNCs cyclohexane solution was added into the above mixture. The resultant solution was magnetically stirred for 30 min, and then 0.4 mL of (28 wt%) ammonium hydroxide solution was added to form a reverse microemulsion solution. After stirring for 1h, 0.3 mL of TEOS was added, and the resultant reaction was aged for 14 h under stirring. The final product of $NaLuF_4$: Gd, Yb, Tm@SiO_2 nanoparticles were collected by centrifuging and washed by water and ethanol several times.

2.4. Preparation of $NaLuF_4$: Gd, Yb, Tm@SiO_2@Ag

The obtained $NaLuF_4$: Gd, Yb, Tm@SiO_2 nanoparticles were dispersed into a 10mL mixture solution of ethanol/wate with ultrasonic stirring for 30min. Then 0.130mL APTES was added into the mixture and magnetic stirred for 10min. After that, 0.0153g $AgNO_3$ dispersed into 10ml deionized water was added into the mixture solution under magnetic stirring and kept stirring for 20min. Then, 0.0174g sodium citrate was added into the mixture and the temperature was raised to

100°C and kept for 20min. After the mixture was cool down to room temperature, the obtained $NaLuF_4$: Gd, Yb, Tm@SiO_2@Ag nanocomposite particles were separated by centrifugation and washed with water and ethanol three times. The final product was dispersed in 20ml ethanol.

2.5. Preparation of $NaLuF_4$:Gd,Yb,Tm@SiO_2@Ag@TiO_2

$NaLuF_4$: Gd，Yb, Tm@Ag@SiO_2 (0.5 mmol) was dispersed in 20 mL of alcohol by sonication treatment. Then, 0.1 g of HPC and 0.1 mL of deionized water were added into the suspension, followed by magnetic stirring for 2 h at room temperature to ensure the sufficient adsorption of hydroxypropyl cellulose by $NaLuF_4$:Gd，Yb,Tm@ Ag@ SiO_2. 1mL of tetrabutyl titanate was added into 5 mL of alcohol to form a transparent solution which was then added into the suspension drop by drop with a speed of 0.5 mL/min. After that, the temperature was raised to 85° C under refluxing conditions for 100 min. The precipitate was isolated by centrifugation, washed with ethanol, and dispersed in 33mL of ethanol to give a $NaLuF_4$:Gd,Yb,Tm@Ag@SiO_2@amorphrousTiO_2 suspension. The as-obtained $NaLuF_4$:Gd,Yb,Tm@SiO_2@Ag@amorphrousTiO_2 suspension was mixed with 17 mL of deionized water by sonication and magnetic stirring for 30 min. The resulting suspension was transferred to a Teflon-lined stainless steel autoclave and heated at 180° C for 24 h in an electric oven. After the reaction, the product was collected by centrifugation and washed with deionized water and ethanol for three times, and then dried at 60 °C in a vacuum oven.

2.6. Characterizations

The sizes and morphologies of prepared products were characterized with a JEOL JEM-2010F transmission electron microscope (TEM) operating at 200 kV. Energy-dispersive X-ray analysis (EDX) of the samples was performed during high-resolution transmission electron microscopy (HRTEM) measurements to determine the elements of the samples. The crystal phase structures of the as-prepared samples were examined by powder X-ray diffraction (XRD) measurements that were performed on a Rigaku D/max-2500 X-ray diffractometer using Cu Kα radiation. The scan was performed in the 2θ range from 10° to 80° with a scanning rate of 8°/min. The upconversion luminescence spectra were recorded with an Edinburgh FLS-920 fluorescence spectrophotometer using an external 0-2 W adjustable laser (980 nm, Beijing Hi-Tech Optoelectronic Co., China) as the excitation source instead of the Xenon source in the spectrophotometer. UV-vis absorption spectra were measured on a Hitachi 3010 UV-vis spectrophotometer (Japan).

2.7. Photocatalytic Experiments.

Photocatalysis was performed via monitoring RhB degradation by measuring the variation of optical absorption of RhB with a Hitachi U-3010 spectrophotometer, using SGY-IB multifunction of photochemical reactor (Nanjing Sidongke Electri Co. Ltd.) as photocatalytic reaction device. In a typical experiment, 20 mg of sample (catalyst) was dispersed into a quartz cuvette containing 50 mL of RhB aqueous solution (20 mg/L). The suspension was magnetically stirred in the dark for 30 min to attain adsorption-desorption equilibrium between dye and catalyst. Then the photoreaction vessels were exposed to the simulated solar light irradiation produced by a 500 W Xe lamp（PL-X500D） (the wavelength distribution is similar to the solar light). At giving time intervals, the photoreacted solutions were analyzed by recording variations of the absorption band

maximum (554 nm) in the UV-Visible spectra of RhB.

The degradation ratio η (%) of dye was calculated using the following equation:

$$\eta\ (\%) = [\ (C_0\text{-}C)\ ]/C_0 \times 100$$

$$= [\ (A_0\text{-}A)\ ]/A_0 \times 100$$

Where C_0 and C are the initial and residual concentrations of RhB in solution resepctively, and A_0 and A are the absorbance of RhB at 554nm before and after exposing under simulated solar light respectively.

3. RESULTS AND DISCUSSION

The fabrication of the sandwich structure is depicted in Scheme 1. The UCNCs of $NaLuF_4$: Gd, Yb, Tm was first synthesized through a thermal decomposition method.[38] A layer of amorphous SiO_2 as the media shell was generated outside the UCNCs through reverse microemulsion method.[39] Ag nanoparticles generated by reduction of $AgNO_3$ using citrate sodium as reductant were immobilization on the surface of the SiO_2 shell through a chemical affinity towards primary amines.[40] The primary amine originally acts as a ligand coming from APTES which was introduced during the synthetical process. In the presence of HPC, the UCNCs@SiO_2@Ag composite were over coated with a layer of TiO_2 by hydrolyzing tetrabutyl orthotitanate (TBOT) in ethanol solution.[29] The outer TiO_2 shell is composed of a layer amorphous TiO_2 before annealing, or a large amount of tiny nanoparticles of anatase TiO_2 after hydrothermally annealing at 180° C for 24 h.

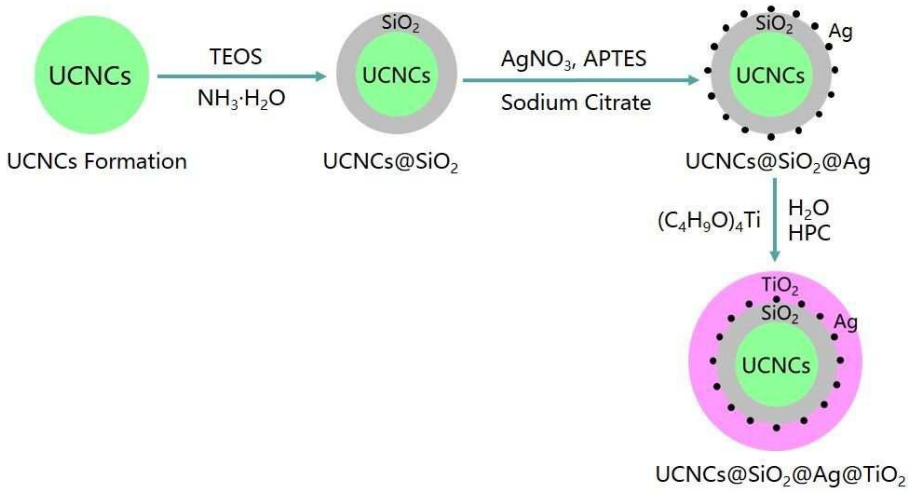

Scheme 1. Schematic illustration of the fabrication process of the sandwich-structured UCNCs@SiO_2@Ag @TiO_2 photocatalyst.

3.1. Phase and Morphology Characterization

Fig.1 shows the X-ray diffraction (XRD) patterns of the prepared products. As shown in Fig. 1，all of the samples show the same characteristic diffraction peaks (100, 110, 101, 200, 111, 210, 002, 211, 102, 112 and 200), which match well with the standard card of typical hexagonal phase of $NaLuF_4$ (JCPDS: 27-0726).[26, 41] Both of UCNCs@SiO_2@Ag and UCNCs@SiO_2@Ag@TiO_2 (Fig. 1b and 1d) show typical face-centered cubic phase of silver (JCPDS 87-0720),[29] confirming the formation of Ag nanoparticles. As shown in the XRD patterns of UCNCs@SiO_2@TiO_2 and UCNCs@SiO_2@Ag@TiO_2 (Fig.1c and 1d), the characteristic diffraction peaks of TiO_2 are observed which are assigned to anatase titania according to the JCPDS No. 21-1272,[42] confirming the formation of a layer of anatase TiO_2.

The TEM images of prepared products are shown in Fig. 2. As shown in Fig. 2a, $NaLuF_4$: Gd,

Yb, Tm nanocrystals are hexagonal plate-liked structure with diameter about 46 nm, which are well-dispersed and uniform in morphology and size. The TEM images of $NaLuF_4$: Gd,Yb,Tm@SiO_2 (Fig. 2b), $NaLuF_4$: Gd,Yb,Tm@SiO_2@Ag (Fig. 2c), $NaLuF_4$: Gd,Yb,Tm@SiO_2@Ag@amorphous TiO_2 (Fig. 2d) and $NaLuF_4$: Gd,Yb,Tm@SiO_2@Ag@TiO_2 (Fig. 2d) show that the surface structure was changed remarkable when the UCNCs was incorporated with SiO_2, Ag and TiO_2 to form different composites. Fig. 2b shows a light and smooth layer of SiO_2 with thickness of 24.5nm is coated onto the surface of the UCNCs. Fig. 2c shows the Ag nanoparticles (15nm) are formed and attached on the surface of SiO_2. Fig. 2d and 2e show the out layer of amorphous TiO_2 before annealing and a large amount of tiny nanoparticles of anatase TiO_2 after hydrothermally annealing, respectively. These small sized TiO_2 nanoparticles dispersed around the surface of $NaLuF_4$:Gd, Yb,Tm@SiO_2@Ag will result in a large internal surface area which can enhance the contact with contaminants for efficient photocatalytic degradation.[43, 44] The HRTEM images of $NaLuF_4$: Gd, Yb, Tm (Fig. 2a, inset), Ag (Fig. 2c, inset) and TiO_2 (Fig. 2e, inset) reveal highly crystalline natures of the as-prepared products. The interplanar distances between adjacent lattice fringes correspond to the crystal planes of the nanocrystals, good agreeing with the XRD detected results. The measured values of the interplanar distances are similar to the literatures and our previous reports.[18, 27, 29, 43]

The composition of $NaLuF_4$: Gd, Yb,Tm@SiO_2@Ag@TiO_2 was characterized by EDX analysis. As shown in Fig. 2f, all of the elements including Na, Lu, F, Gd, Yb, Tm, Ti, Ag, Si and O were detected, further confirmed the formation of the nanocomposite photocatalyst.

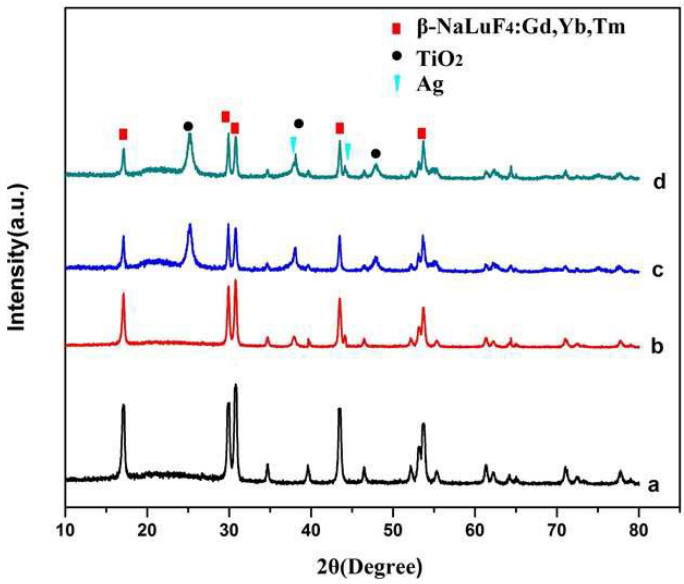

Fig. 1. XRD patterns of $NaLuF_4$:Gd,Yb,Tm (a), $NaLuF_4$:Gd,Yb,Tm@SiO_2@Ag (b), $NaLuF_4$:Gd,Yb,Tm@SiO_2@TiO_2(c), and $NaLuF_4$: Gd,Yb,Tm@SiO_2@Ag@TiO_2 (d).

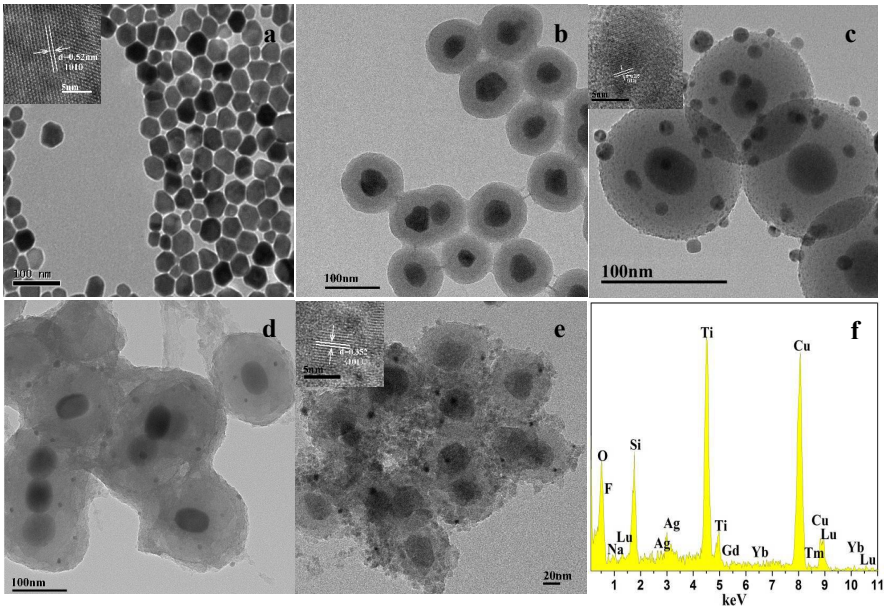

Fig. 2 TEM images of the $NaLuF_4$:Gd,Yb,Tm(a), $NaLuF_4$:Gd,Yb,Tm@SiO_2 (b), $NaLuF_4$: Gd,Yb,Tm@SiO_2 @Ag (c), $NaLuF_4$:Gd,Yb,Tm@SiO_2@Ag@amorphrous TiO_2 (d), and $NaLuF_4$:Gd, Yb,Tm@SiO_2@Ag@TiO_2 (e). HRTEM images of $NaLuF_4$:Gd,Yb,Tm (1a, inset), Ag (1c, inset) and TiO_2(1e, inset). EDX spectra of $NaLuF_4$:Gd,Yb, Tm@SiO_2@Ag@TiO_2

3.2. UV−vis-NIR Absorption Spectra Analysis

UV−vis-NIR absorption spectra of TiO_2, $NaLuF_4$: Gd, Yb, Tm nanocrystal and $NaLuF_4$: Gd, Yb, Tm@SiO_2@Ag@TiO_2 nanocomposite are shown in Fig.3. TiO_2 and $NaLuF_4$: Gd, Yb, Tm@SiO_2@Ag@TiO_2 have sharp peaks emerging at ~400 nm corresponding to the band-gap absorption of TiO_2.[43] Based on the spectra, it can be speculated that the UV photos generated from the upconversion process of $NaLuF_4$:Gd,Yb,Tm can be absorbed by the anatase TiO_2 *via* an energy transfer. $NaLuF_4$: Gd, Yb, Tm@SiO_2@Ag@TiO_2 shows a absorption band at wavelengths of 350-500nm, which is localized surface plasmon resonance (LSPR) absorption of Ag nanoparticles, similar to the values reported in our previous studies and literatures.[29, 45] The LSPR of Ag nanoparticles can help the nanocomposite photocatalyst to harvest the visible light energy. The appearance of LSPR peak confirms the Ag nanoparticles have been successfully embedded in the as-prepared nanocomposite.[46] Both of $NaLuF_4$:Gd,Yb,Tm and $NaLuF_4$: Gd, Yb, Tm@SiO_2@Ag@TiO_2 have an absorption peak at 980nm which is attributed to the adsorption of Yb^{3+} ions.

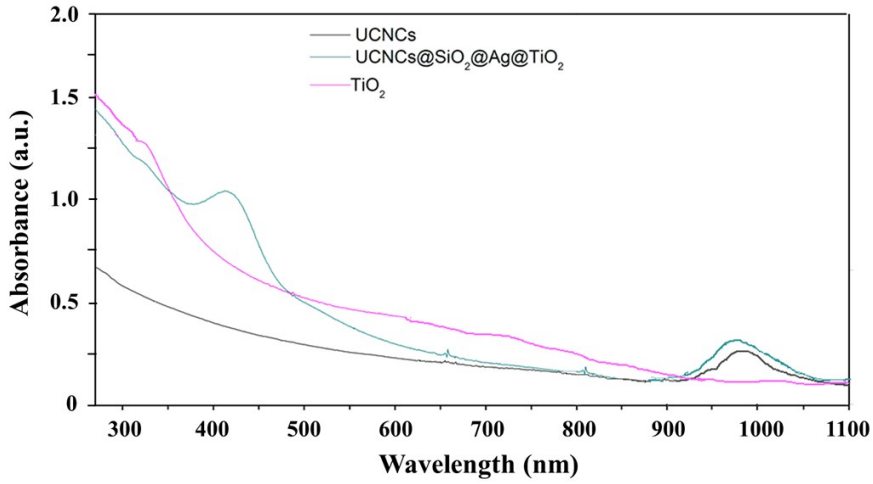

Fig. 3 UV−vis-NIR absorbance spectra of the products

3.3. Upconversion Luminescence Properties of the Nanocomposite

Fig.4 shows the upconversion luminescence (UCL) spectra of the as-prepared products. The UCL intensities of the samples were measured at the same concentration of 1.0mg/ml in cyclohexane. It can be seen that each of them shows typical characteristic UCL of Tm^{3+} under CW excitation at 980nm. The UV emission peaks centered at 361 nm is attributed to the transitions of Tm^{3+} ions: $^1D_2 \rightarrow {}^3H_6$.[43,47] A very weak UV emission peak at 310nm originated from the transition $^6P_{7/2} \rightarrow {}^8S_{7/2}$ of Gd^{3+} ions.[48] The visible emission peaks at 450 nm, 476 nm, 645nm and 697nm are assigned to $^1D_2 \rightarrow {}^3H_4$, $^1G_4 \rightarrow {}^3H_6$, $^1G_4 \rightarrow {}^3F_4$ and $^3F_3 \rightarrow {}^3H_6$ transitions of Tm^{3+} ions, respectively.[47, 49]

Fig. 5 shows the possible upconversion luminescence mechanisms in the system. Under the 980nm excitation, the Yb^{3+}ion is excited from $^2F_{7/2}$ to $^2F_{5/2}$ level and then drops back to the ground state, with transfer of the energy to the adjacent Tm^{3+} ion to excite it from the $^3H_6$ ground state to the $^3H_5$ excited state: $^2F_{5/2}$ (Yb^{3+}) + $^3H_6$ (Tm^{3+}) → $^2F_{7/2}$ (Yb^{3+}) + $^3H_5$ (Tm^{3+}), populating the $^3F_4$ state by nonradiative relaxation. Likewise, Tm^{3+} ions are excited to the $^3F_{2,3}$ and $^1G_4$ state in turn. The $^1D_2$ state is populated by the cross-relaxation progress $^3F_3 \rightarrow {}^3H_6$: $^3F_3 \rightarrow {}^1D_2$ (Tm^{3+}). Furthermore, with the help of another excited Yb^{3+} ion, the Tm^{3+} ion is promoted from the $^1D_2$ state to $^3P_2$ state, and then populates the $^1I_6$ state by nonradiative relaxation.[50] For the large energy gap between the ground state $^8S_{7/2}$ and excited state ^6I_J of Gd^{3+} ion, the Gd^{3+} cannot absorb 980nm photons directly. However, the excited states ^6I_J of Gd^{3+}can be populated through the energy transfer $^3P_2 \rightarrow {}^3H_6$ (Tm^{3+}): $^8S_{7/2} \rightarrow {}^6I_J$ (Gd^{3+}). Subsequently, at room temperature, the non-radiative relaxation $^6I_J \rightarrow {}^6P_J$ is larger than the radiative transition of $^6I_{7/2} \rightarrow {}^8S_{7/2}$, which results in populating $^6P_{7/2}$ level.[51]

The luminescence intensity of $NaLuF_4$: Gd, Yb, Tm@SiO_2 decreases to some extent in comparison to that of pure $NaLuF_4$: Gd, Yb, Tm due to the light scattering effects by the silica layer.[52] However, the coated SiO_2 shell serves as an interface for Ag decoration and an isolating layer to prevent fluorescence quenching induced by energy transfer from UCNCs to the metal Ag.[52] Furthermore, this SiO_2 layer will also prevent the electron trapping caused by surface defects and ligands of bare $NaLuF_4$: Gd, Yb, Tm,[53] and prevent the upconversion nanoparticles from photocatalysis induced corrosion to prolong its lifetime.[44] In comparison to bare $NaLuF_4$: Gd, Yb, Tm and $NaLuF_4$: Gd, Yb@SiO_2, the UCL intensity of $NaLuF_4$: Gd, Yb@SiO_2@Ag increases a lot. This fluorescence enhancement is attributed to the metal-enhanced fluorescence (MEF) of Ag nanoparticles. MEF arises from the interaction between fluorophore and surface plasmon resonance (SPR) of metal nanoparticles.[54] SPR is the collective electron-cloud oscillation on a noble metal surface, caused by the interaction of the noble metal with incident light.[54,55] A key aspect of the SPR effect is increase in the intensity of the local electric field in the proximity of metal nanoparticles, which can significantly modify the spectroscopic properties of neighboring fluouophores.[56] In addition, the interaction between fluorophore and SPR of metal nanoparticles can increase the emission rate of the fluorophore by surface plasmon-coupled emission (SPCE).[43]

The theory of MEF has been developed since the 1980s,[57] in which the effects are attributed to at least two known mechanisms.[57, 58] One is an increase in the emission intensity as a result of the SPR increasing the local electric field on the fluorophore, E_m. This effect will result in increased intensities, but the lifetime and quantum yield of the fluorophore will be unchanged. This fluorescent enhancement can be understood as being due to the metal particles that concentrate the local electric field and subsequently increase the rate of excitation.[59] The maximum enhancement

of fluorescence emission is achieved if the SPR wavelength equals the absorption wavelength of fluorophores.[59] The second mechanism is that a nearby metal can increase the intrinsic radiative decay rate of the fluorophore, Γ_m, resulting in increasing quantum yield and emission intensity of the fluorophore.[60] The maximum enhancement of fluorescence emission is achieved if the SPR wavelength equals the emission wavelength of fluorophores.[60]

In our case, Ag nanoparticles are embedded inside the nanocomposite, which are near the fluouophore of $NaLuF_4$: Yb, Gd, Tm. The local electric field drastically increases induced by the SPR of the Ag nanoparticles, which leads to the increase in excitation rates as well as emission intensity of the UCNCs. Furthermore, as shown in Fig. 3 and Fig. 4, the plasmon resonance frequency of the Ag nanoparticles overlaps well with the emission band of UCNCs. This allowing an effective SPCE will result in an increasing emission rate as well as emission intensity of the UCNCs.[61] We suggested that the SPCE played an important role in the spectra-dependent enhancement of upconversion emission, although other effects such as local electric field enhancement might also contribute to the enhancement. Thus, the emission enhancement in the present study could be attributed to two possible factors: 1) an increase in the excitation rate by local electric field enhancement, that is, an enhancement of the effective excitation flux caused by the local electric field enhancement associated with SPR; 2) an increase in the radiative decay rate of the fluorophore by surface plasmon-coupled emission (SPCE).

After further TiO_2 coating, the luminescence intensity decreases significantly in comparison to the $NaLuF_4$: Gd, Yb, Tm@SiO_2@Ag. The lights in UV region emitted by UCNCs are nearly disappear, which is attributed the absorbance of TiO_2 shell caused by a energy transfer process between UCNCs and TiO_2.[34] The lights in visible region for $NaLuF_4$: Gd, Yb,

$Tm@SiO_2@Ag@TiO_2$ are also decreased, which can be assigned to the shielding effect of TiO_2 shell.[62]

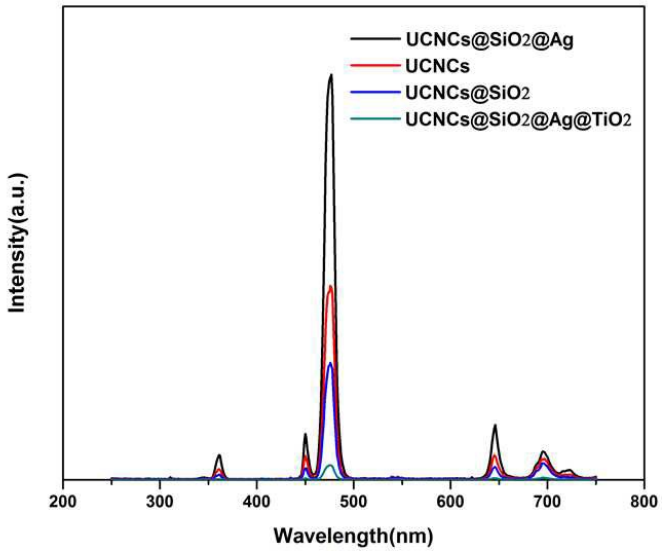

Fig. 4 Upconversion luminescence spectra of the products under 980 nm excitation

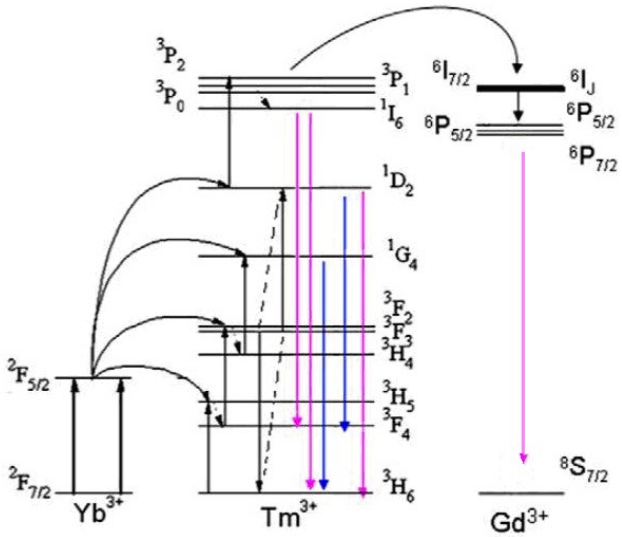

Fig. 5 Energy levels and upconversion luminescence scheme for $NaLuF_4$: Gd, Yb, $Tm@SiO_2@Ag@TiO_2$

3.4. Photocatalytic Measurements

RhB was used as a model pollutant to investigate the photocatalytic activity of $NaLuF_4$: Gd, Yb, Tm@SiO_2@Ag@TiO_2 nanocomposite. A 500 W xenon lamp (wavelength distribution: 300-2500 nm) was used as simulated solar light for light source. Upon irradiation for a designated time, 1mL RhB aqueous solution was taken out and diluted to 4 mL for absorbance measurement. Fig. 6 shows the absorbance spectra of RhB catalyzed by the $NaLuF_4$:Gd,Yb,Tm@SiO_2@Ag@TiO_2 nanocomposite under simulated solar light irradiation as a function of the irradiation time. The absorption intensity of RhB at 554nm decreases gradually with the increase of irradiation time, indicating the degradation of RhB upon the simulated solar light irradiation.

The photocatalytic efficiency of the nanocomposite can be evaluated through calculating the time-depended degradation ratio of dye with contrast in P25, TiO_2, $NaLuF_4$:Gd,Yb,Tm，SiO_2@Ag@TiO_2 and $NaLuF_4$: Gd, Yb, Tm@SiO_2@TiO_2. Fig. 7 shows the time profile of C/C_0 under simulated solar light irradiation, where C is the concentration of RhB at the irradiation time and C_0 is the concentration of adsorption equilibrium with the photocatalysts before irradiation.

It can be seen from Fig. 7, the photocatalytic efficiency of $NaLuF_4$: Gd, Yb, Tm@SiO_2@Ag@TiO_2 nanocomposite is obviously higher than that of controls. The RhB is almost completely degraded (99.46%) in the present of $NaLuF_4$: Gd, Yb, Tm@SiO_2@Ag@TiO_2 after exposed under Xe lamp for 210min, whereas the degradation ratios of $NaLuF_4$: Gd, Yb, Tm@SiO_2@TiO_2, SiO_2@Ag@TiO_2, TiO_2 and P25 are only 83.98%, 62.66%, 26.32% and 31.28%, respectively. The photocatalytic activity of $NaLuF_4$: Gd, Yb, Tm@SiO_2Ag@TiO_2 is higher than that of SiO_2@Ag@TiO_2, which can be assigned to the function of $NaLuF_4$: Gd, Yb, Tm. The

UCNCs of $NaLuF_4$: Gd, Yb, Tm can absorb the NIR region light and convert it into UV and visible light, in which the UV light can be absorbed by TiO_2. By utilizing the UCNCs, NIR irradiation can be absorbed and harvested indirectly by TiO_2 to broaden the absorption region and consequently enhance photocatalytic activity of TiO_2.[36] In addition, when the high energetic UV photons supplied by UCNCs are absorbed by the TiO_2 it can drive the TiO_2 to generate high energetic electron and hole pairs.[43] These high energetic electron and hole pairs possessing high oxidation-reduction abilities should exhibit high catalytic activity.[34] The photocatalytic activity of SiO_2@Ag@TiO_2 is higher than that of P25 and TiO_2, and $NaLuF_4$: Gd, Yb, Tm@SiO_2@Ag@TiO_2 is higher than that of $NaLuF_4$: Gd, Yb, Tm@SiO_2@TiO_2, which can be attributed to the function of Ag nanoparticles. The Ag nanoparticles presented in the composite have three functions: 1) to significantly enhance the upconversion luminescence of UCNCs caused by its metal-enhanced fluorescence effect, which can make a better use of UCNCs as upconversion luminescent centers in the composite. 2) to enhance separation of photogenerated electrons and holes of TiO_2 by serving as an electron reservoir.[35] It is well-known that the noble metal Ag can act as effective electron acceptor and transporter, trapping the photogenerated electorns, thereby improving the separation of electron-hole pairs and inhibition of recombination of electron-hole pairs.[36] 3) to help harvesting the visible light energy by its phasmonic properties.[37] As shown in Fig. 3, the nanocomposite photocatalyst $NaLuF_4$: Gd, Yb, Tm@SiO_2@Ag@TiO_2 has an absorption band at 350-500nm aroused by the LSPR of Ag nanoparticles. The Ag nanoparticles act as light harvesting components *via* excitation of their LSPR in the visible range of spectrum.[52]

The degradation kinetics of photocatalysis usually fit the Langmuir–Hinshelwood (L–H) model (Eq. 1),[63] according to which the rate of the photocatalytic reaction r is proportional to the

fraction of the surface covered by the organic substrate (θ_x):

$$r = -\frac{dc}{dt} = k\theta_x = k\frac{Kc}{1+Kc} \qquad (1)$$

where *k* is the apparent reation rate constant, c is the concentration of the organic species, and K is the Langmuir adsorption constant.

When the concentration is low (i.e. Kc « 1), Eq. (1) can be simplified to a pseudo-first-order kinetic law (Eq. 2):[63]

$$-\frac{dc}{dt} = -kc \qquad (2)$$

The linear plots of $-\ln(c/c_0)$ vs. time, are shown in Fig.8. According to the plots, the apparent rate constants were calculated as 1. 979×10^{-2}, 9.04×10^{-3}，5.23×10^{-3}，$1.66\times10^{-3}$and 1.94×10^{-3} min^{-1} for $NaLuF_4$: Gd, Yb, Tm@SiO_2@Ag@TiO_2 nanocomposite, $NaLuF_4$: Gd, Yb, Tm@SiO_2@TiO_2 nanocomposite, SiO_2@Ag@TiO_2 nanocomposite, TiO_2 and P25, respectively. Usually, a high apparent rate constant indicates a high caltalytic reaction rate and a high catalytic activity of the catalyst.[26,29] The degradation rate of $NaLuF_4$: Gd, Yb, Tm@SiO_2@Ag@TiO_2 nanocomposite is about 10 times higher than that of P25. The high apparent rate constant of $NaLuF_4$: Gd, Yb, Tm@SiO_2@Ag@TiO_2 further demonstrates its high photocatalytic activity.

In order to further confirm the contribution from upconversion materials, a test of photocatalytic degradation under NIR (980nm) irradiation was performed. The obtained results are shown in Fig.9. Similar to the results obtained under simulated solar irradiation, the RhB is almost completely degraded in the present of $NaLuF_4$: Gd, Yb, Tm@SiO_2@Ag@TiO_2 after exposing under 980nm light for 210min, and it is much higher than that of controls. These results demonstrate that the as-prepared photocatalyst of $NaLuF_4$: Gd, Yb, Tm@SiO_2@Ag@TiO_2 also has high photocatalytic activity under NIR irradiation in comparison to the controls, further

confirming the contribution of the upconversion materials and the advantage of the as-prepared product.

The as-prepared nanocomposite exhibited high photocatalytic activity. Moreover, as UCNCs, TiO_2, Ag@SiO_2@UCNCs and UCNCs@SiO_2@Ag having no toxicity,[26,29] it can be deduced that the nanocomposite should have no toxicity to organism and environmental. The prepared product is predicted as a potential catalyst to be used for environmental cleaning.

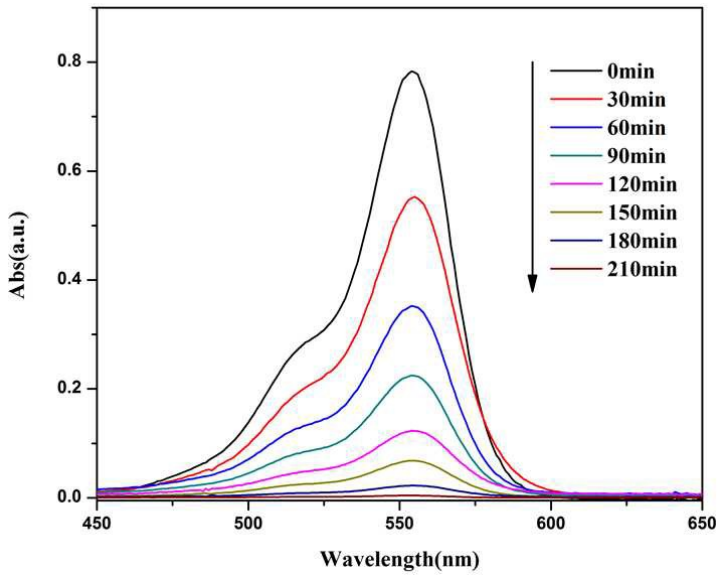

Fig. 6 Absorbance spectra of RhB catalyzed by the $NaLuF_4$: Gd, Yb, Tm@SiO_2@Ag @TiO_2 nanocomposite at different irradiation times under stimulated solar light irradiation

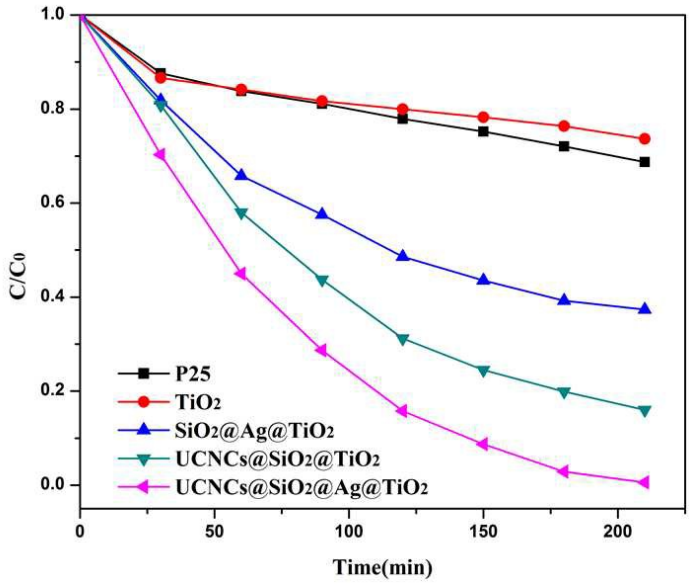

Fig. 7 Photocatalytic degradation of RhB under stimulated solar light irradiation

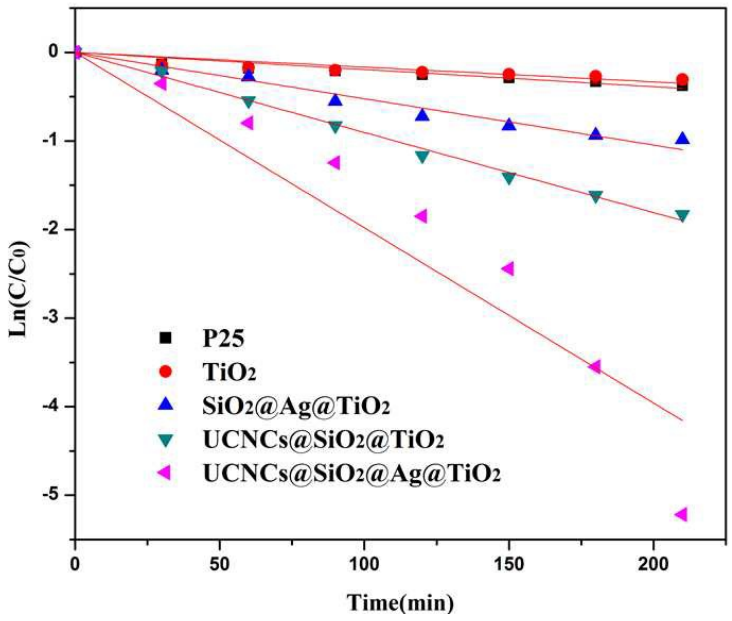

Fig.8 Kinetics of RhB degradation under stimulated solar light irradiation

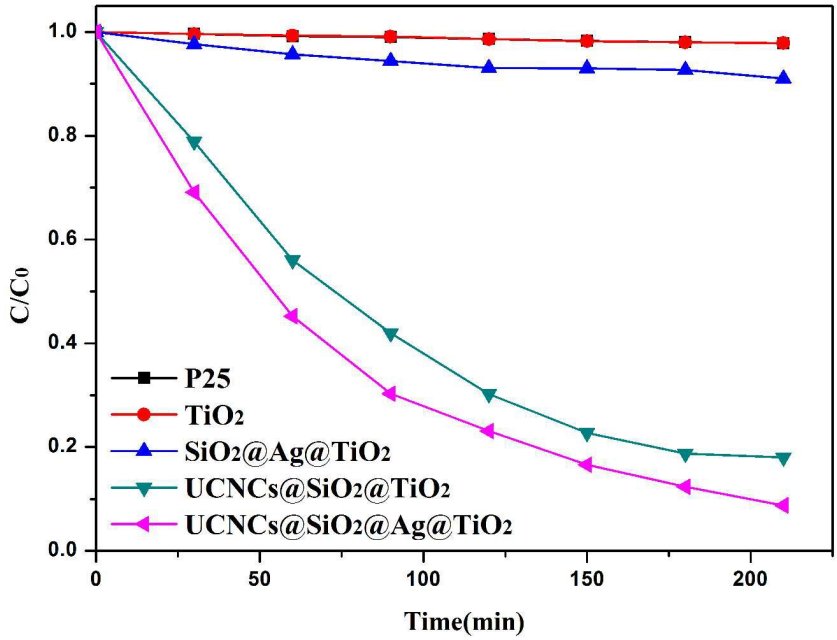

Fig.9 Photocatalytic degradation of RhB under NIR irradiation

The physical process of the photocatalysis is shown in Fig.10. As shown in Fig.10, the outer TiO_2 layer can quickly absorb the UV from solar lights for its intrinsic property. The high penetrability of the NIR from the solar light allows it to go further into the inner to excite the upconversiont nanocrystals $NaLuF_4$: Gd, Yb, Tm emitting UV and visible lights. Then the upconverted UV light will pass through the transparent SiO_2 layer to excite the outer TiO_2 nanocrystals. After absorbing the solar and upconverted lights, the excited TiO_2 generates electron-hole pairs. These electron-hole pairs then migrate from inner region to the surfaces and act as catalytic centre. These electrons and holes can not only directly decompose the pollutant, but also degrade the pollutant indirectly through $\cdot OH$ and $\cdot O_2^-$ radicals that are produced from oxidizing H_2O and reducing O_2 molecules by the holes and electrons, respectively.[34]

As shown in Fig.10, the excited electrons arriving on the surface react with the oxygen adsorbed on the surface of TiO_2 to form O^{2-} or O_2^{2-}, which combines with H^+ to form hydrogen peroxide (H_2O_2).[64] H_2O_2 reacts with superoxide radical anion ($\cdot O_2^-$) to generate hydroxyl radical ($\cdot OH$).[65] These reactive oxygen species ($\cdot OH$, $\cdot O_2^-$ and H_2O_2), especially $\cdot OH$ and $\cdot O_2^-$, could directly take part in the photocatalytic degradation reaction to degrade RhB. The processes are presented as following equations.

$TiO_2 + \hbar\nu \rightarrow e^- + h^+$

$h^+ + H_2O_2 \rightarrow H^+ + \cdot OH$

$e^- + H^+ + O_2 \rightarrow H_2O_2$

$e^- + O_2 \rightarrow \quad \cdot O_2^-$

$\cdot O_2^- + H_2O_2 \rightarrow \cdot OH + OH^- + O_2$

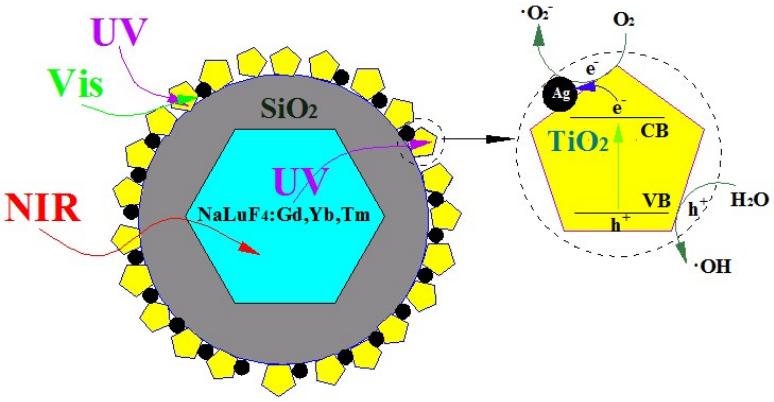

Fig.10. Illustrative diagrams of photocatalytic mechanism of $NaLuF_4$: Gd, Yb, Tm@SiO_2@Ag @TiO_2 photocatalyst under solar light irradiation

4. CONCLUSIONS

In summary, a novel nanocomposite photocatalyst $NaLuF_4$: Gd, Yb, Tm@SiO_2@Ag @TiO_2 was synthesized successfully. The prepared catalyst showed a high efficiency in catalyzing decomposition of dye RhB under illumination of stimulated solar light. Its photocatalytic activity was significant higher than that of pure TiO_2 and P25. The structural design of the photocatalyst takes advantage of the synergetic synergistic effect of UCNCs and Ag nanoparticles. The excellent photocatalytic efficiency can be attributed to the UCNCs, which convert NIR into UV and indirectly extend the light response range of TiO_2, to the Ag nanoparticles, leading to enhance light harvesting and charge separation. This work presented a new strategy to significantly improve the photocatalytic activity of TiO_2 under solar light irradiation by artificial integrating UCNCs and noble metal with TiO_2 into a hetero-composite nanostructure.

Corresponding Author

*Address: 608 Room, School of Environmental and Chemical Engineering, Shanghai University, Shanghai 200444, China. Phone: 86-21-66137502. Fax: 86-21-66137787. E-mail: ydg@shu.edu.cn.

Notes

The authors declare no competing financial interest.

ACKNOWLEDGMENTS

The authors acknowledge the National Natural Science Foundation of China (No. 21271126, 11025526), Program for Innovative Research Team in University (No. IRT 13078), and National 973 Program (No.2010CB933901).

REFERENCES

1 G. Wang, Y. Ling and Y. Li, *Nanoscale,* 2012, **4**, 6682.

2 R. Chalasani and S. Vasudevan, *Acs. Nano*., 2013, **7**, 4093.

3 T. Fotiou, T. M. Triantis, T. Kaloudis and A. Hiskia, *J. Chem. Eng.,* 2015, **261**,17.

4 L. Gao, J. Zhang, C. He, Y. Zhang, Q. J. Sun and Y. F. Li, *Sci. China. Chem.*, 2014, **57**,966.

5 A. Sadhana Sawant, P. Savita Somani, H. Arati Jadhav, A. Nene, S. K. Omanwar and R. Prakash Somani, *J. Green Sci. Technol.,*2013, **1**, 2.

6 X. Yang, J. Qin, Y. Jiang, R. Li, Y. Li and H. Tang, *Rsc. Adv.,* 2014, **4**,18627.

7 R. Varshney, S. Bhadauri and S. G. Mulayam, *Nano. Biomed. Eng.,* 2012, **4**,99.

8 S. C. Yan, L. Y. Zhou, Y. Shi, Z. L. Cao, D. Hu and X. Xu, *J. Green Sci. Technol.,*2013,**1**, 131.

9 M. Shamalah, R. S. L. Aparna, R. G. S. V. Prasad, and A. R. Phani, *J. Green. Sci. Technol.,*2013,**1**, 14.

10 M. Koelsch, S. Cassaignon, C. T. T. Thanh Minh, J. F. Guillemoles and J. P. Jolivet, *Thin Solid Films.,*2004, **451** , 86.

11 G. Liu, Y. N. Zhao, C. H. Sun, F. Li, G. Q. Lu and H. M. Cheng, *Angew. Chem.,* 2008, **47**,4516.

12 H. X. Shi, T. X. Zhang, T. C. An, B. Li and X.Wang, *J. Colloid. Interf. Sci.,* 2012,**380**,121.

13 S. Kango, S. Kalia, A. Celli, J. Njuguna, Y. Habibi and R. Kumar, *Prog. Polym. Sci.,* 2013, **38**, 1232.

14 J. F. Yanab and F. *J.* Zhou, *Mater. Chem.,* 2011, **21**, 9406.

15 Y. Huo, J. Zhu, J. Li, G. S. Li and H. X. Li, *J. Mol. Catal. A: Chem.*, 2007, **278**, 237.

16 Z. Liu, B. Guo, L. Hong and H. X. Jiang, *J. Phys. Chem. Solids.*, 2005, **66**,161.

17 M. Sathish, B. Viswanathan, R. P. Viswanath and S. G. Chinnakonda, *Chem. Mater.,* 2005, **17**,6349.

18 W. Fan, S. Jewell and Y. She, *Phys. Chem. Chem. Phys*., 2013, **16**, 676.

19 J. Xu, W. Wang, S. Sun and L. Wang, *Appl. Catal. B: Environ.,* 2012, **111**, 126.

20 S. Kohtani, E. Yoshioka and H. Miyabe, *Intechopen*.,2012, **101**, 12288.

21 S. Lee, I. Cho and Y. Sohn, *J. Nanosci. Nanotechnol.,* 2015,**15**, 8362.

22 M. He , O. Huang, C. L. Zhang, and F. Chen, *Chem .Comm.,* 2011, **47**,9510.

23 T. Wang, L. Wang, L. M. Zhang, Z. X. Lu, L. L. Guo, L. Wang, Z. F. Wang, N. Y. He, C. R. Zhou and L. Huang, *J. Nanosci. Nanotechnol.,* 2015,**15**, 6734.

24 L. M. Zhang, Z. X. Wang, Z. X. Lu, K. Xia, Y. Deng, S. Li, C. X. Zhang, Y. F. Huang and N. Y. He, *J. Nanosci. Nanotechnol.,*2014,**14**, 4710.

25 Q. Liu, Y. Sun, T. S. Yang, W. Feng, J. Wang, C.G. Li and F. Y. Li, *J. Am. Chem. Soc.*, 2011, **133**,17122

26 D. G. Yin, X. Z Cao, L.Zhang, J. X. Tang, W. F. Huang,Y. L. Han and M. H. Wu, *Dalton. T.,* 2015, **44**, 11147.

27 J. Ouyang, D. G. Yin, X. Z. Cao, C. C. Wang, K. L. Song, B. Liu, L. Zhang, Y. L Han and M. H. Wu, *Dalton. T.*, 2014, **43**,14001.

28 Z. H. Chen, X. F. Wu, S. G. Hu, P. H, H. Y. Yan, Z. G. Tang and Y. X. Liu, *J. Mater. Chem.C.,* 2015, **3**, 153

29 D. G. Yin, C. C. Wang, J. Ouyang, X. Y. Zhang, Y. Feng, K. L. Song, B. Liu, X. Z. Cao, L. Zhang, H. Y. Lin and M. H. Wu, *ACS Appl. Mater. Inter.*, 2014, **6**, 18480.

30 L. Liu, H. M. Li and J. C. Dai, *Sci. China. Chem.*, 2014, **57**,918.

31 F. Wang, Y. Han, C. S. Lin,Y. H. Lu, J. Wang, J. Xu, H. Chen, C. Zhang, M. H. Hong and X. G. Liu, *Nature*, 2010, **463**, 1061

32 S. Q. Huang, Z. Y. Lou, N. W. Zhu and H. P. Yuan, *Catal. Commun.,* 2015, **61**, 6.

33 G. Y. Shi, Y. F. Mao, G. Z. Ren, L. J. Gong and Z. G. Zhi, *Opt. Commun.,* 2014, **332**, 219.

34 Y. Tang, W. Di, X. Zhai, R. Y. Yang and W. P. Qin, *ACS. Catal.,* 2013, **3**, 405.

35 H. Chen, F. Gao, R. He and D. X. Cui, *J. Colloid. Interf. Sci.,* 2007, **315**, 158.

36 D. G. Yin, L. Zhang, B. H. Liu and M. H, Wu, *J. Nanosci. Nanotechnol.,* 2012, **12**, 2248.

37 D. G. Yin, B. H. Liu, L. Zhang and M.H. Wu, *J. Biomed. Nanotechnol.,* 2012, **8**, 458.

38 F. Vetrone1, R. Naccache, V. Mahalingam, C. G. Morgan and J. A. Capobianco, *Adv. Func. Mater. ,* 2009, **19**, 2924.

39 X. M. Li, L. Zhou, Y. Wei, A. M. El-Toni, F. Zhang and D. Y. Zhao, *J. Am. Chem. Soc.,* 2014, **136**, 15086.

40 J. W. Lee, M. R. Othman, Y. Eom, T. G. Lee, W. S. Kim and J. Kim, *Micropor. Mesopor. Mat.,* 2008, **116**, 561.

41 N. Niu, P. P. Yang, F. He, X. Zhang, S. L. G, C. X. Li and J. Lin, *J. Mater. Chem.*, 2012, **22**,

10889.

42 D. H, Chen, F. Z. Huang, Y. B. Cheng and R. A. Caruso, *Adv. Mater.,* 2009, **21**, 2206.

43 C. C. Wang, K. L. Song, Y. Feng, D. G. Yin, J. Ouyang, B. Liu, X. Z. Cao, L. Zhang, Y. L. Han and M. H. Wu, *Rsc. Adv.*, 2014, **4**: 39118.

44 J. Kummerlen, A. Leitner, H. Brunner, F. R. Aussenegg and A. Wokaun, *Mol. Phys.* 1993, **80**, 1031.

45 J. R. Lakowicz, B. Shen, Z. Gryczynski, S. D'Auria and I. Gryczynski, *Biochem. Bioph. Res. Co.,* 2001, **286**, 875.

46 Y. W. Li, W. D. Ling and Q. F. Han, *J. Alloy.Compd.,* 2015, **633**, 347.

47 N. Liu, W. P. Qin, G. S. Qin, T. Jiang and D. Zhao, *Chem. Commun.*, 2011, 47, 7671.

48 Y. Chen, X. H. Yan , Q. Liu and X. F. Wang, *J. Alloy. Compd.,* 2013, **562**, 99

49 S. H. Tang, J. N. Wang, C. X. Yang, L. X. Dong, D. L. Kong and X. P. Yan, *Nanoscale*, 2014, **6**, 8037.

50 R.J. Thrash and L.F. Johnson, *J. Opt. Soc. Am. B.*,1994, **11,** 881.

51 J. Sytsma, G.F. Imbush and G. Blasse, *J. Phys. Condens. Matter,* 1990, **2**, 5171.

52 P. Zhao, Y. H. Zhu, X. L.Yang, X. Jiang, J. H. Shen and C. Z. Li, *J. Mater. Chem. A*., 2014, **2**, 16523.

53 L. L. Liang, Y. M. Liu, C. H. Bu, K. M. Guo, W. W. Sun, N. Huang, T. Peng, B. Sebo, M. M. Pan, W. Liu, S. S Guo and X. Z. Zhao, *Adv. Mater.* **2013**, 25, 2174.

54 S. Eustis and M. A. El-Sayed, *Soc. Rev.,* 2006, **35**, 209.

55 W. L. Barnes, A. Dereux and T. W. Ebbesen, *Nature*, 2003, **424**, 824.

56 F. Le, D. W. Brandl, Y. A. Urzhumov, H. J. Wang,N. J. Kundu, J. Aizpurua and P. Nordlander, *ACS Nano*., 2008, **2**, 707.

57 A. Camplon, A. R. Gallo, C. B. Harris,H. J. Robota and P. M. Whitmore, *Chem. Phys. Lett.,* 1980, **73**, 447.

58 C. D. Geddes and J. R. Lakowicz, *J. Fluoresc.,* 2002, **12**, 121.

59 W. Wang, W. J. Huang, Y. R. Ni, C. H. Lu and Z. Z. Xu, *ACS. Appl. Mater. Inter.,* 2013, **6**, 340.

60 S. Liu, Z. Zhang and M. Han, *Anal. Chem.*, 2005, **77**, 2595.

61 J. R. Lakowicz, *Anal. Biochem*., 2001, **298**, 1.

62 W. P. Qin, D. S. Zhang, D. Zhao, L. L.Wang and K. Z. Zheng, *Chem. Commun.,*2010, **46**,2304.

63 L. J. Yan ,Y. Cheng ,S. Yuan ,X. J. Yan, X. F. Hu and K.Oh, *Res. Chem. Intermediat.*, 2013,**39**,1673

64 Q. Kang, Q. Z. Lu, S. H. Liu, L. X. Yang, L. F. Wen, S. L. Luo and Q. Y. Cai, *Biomater*., 2010, **31**, 3317.

65 A. Sarkar, A. Shchukarev,A. Leino, K. Kordas, J. Mikkola, P. Petrov, E. Tuchina, A. Popov, M. Darvin, M. Meinke, J. Lademann and V. Tuchin, *Nanotechnology*，2012, **23**, 475711.